

p16^{Ink4a}-induced senescence of pancreatic beta cells enhances insulin secretion

Aharon Helman¹, Agnes Klochendler¹, Narmen Azazmeh¹, Yael Gabai¹, Elad Horwitz¹, Shira Anzi¹, Avital Swisa¹, Reba Condiotti¹, Roy Z Granit¹, Yuval Nevo², Yaakov Fixler¹, Dorin Shreibman¹, Amit Zamir¹, Sharona Tornovsky-Babeay³, Chunhua Dai⁴, Benjamin Glaser³, Alvin C Powers^{4–6}, A M James Shapiro^{7,8}, Mark A Magnuson^{5,9}, Yuval Dor¹ & Ittai Ben-Porath¹

Cellular senescence is thought to contribute to age-associated deterioration of tissue physiology. The senescence effector p16^{Ink4a} is expressed in pancreatic beta cells during aging and limits their proliferative potential; however, its effects on beta cell function are poorly characterized. We found that beta cell-specific activation of p16^{Ink4a} in transgenic mice enhances glucose-stimulated insulin secretion (GSIS). In mice with diabetes, this leads to improved glucose homeostasis, providing an unexpected functional benefit. Expression of p16^{Ink4a} in beta cells induces hallmarks of senescence—including cell enlargement, and greater glucose uptake and mitochondrial activity—which promote increased insulin secretion. GSIS increases during the normal aging of mice and is driven by elevated p16^{Ink4a} activity. We found that islets from human adults contain p16^{Ink4a}-expressing senescent beta cells and that senescence induced by p16^{Ink4a} in a human beta cell line increases insulin secretion in a manner dependent, in part, on the activity of the mechanistic target of rapamycin (mTOR) and the peroxisome proliferator-activated receptor (PPAR)- γ proteins. Our findings reveal a novel role for p16^{Ink4a} and cellular senescence in promoting insulin secretion by beta cells and in regulating normal functional tissue maturation with age.

Aged tissues typically show decreased regenerative capacity and deterioration in overall function. Cellular senescence is thought to contribute to tissue aging and associated pathologies through various means, including the limitation of stem cell proliferation and the secretion of negatively acting paracrine factors^{1,2}. Senescence is often viewed as a stress-response program that is activated in damaged cells, and senescent cells accumulate in aging tissues, as well as in premalignant lesions. Senescence occurs in a variety of additional physiological settings^{1,2}, and it was recently shown to also contribute to embryonic development^{3,4}.

The tumor suppressor protein p16^{Ink4a} (hereafter referred to as p16; encoded from the *CDKN2A* locus) is often transcriptionally activated in cells undergoing senescence and is one of the main regulators of this program⁵. p16 is upregulated in multiple tissues during aging^{6–8} and contributes to age-associated decline in tissue function and regenerative capacity^{9–13}. The main function of p16 is the inhibition of complexes of cyclin D and the cyclin-dependent kinases CDK4 and CDK6, through which it activates the RB1 tumor suppressor protein. RB1, often acting together with p53, induces chromatin modifications that lead to senescence-associated reprogramming of gene expression¹⁴. This results in complex phenotypic changes in

cytoskeletal structure and metabolism—including enhanced protein turnover and secretion, and increased glucose uptake and oxidative phosphorylation^{15–17}. The manner in which senescence affects cell functionality remains poorly understood.

Glucose tolerance deteriorates with age, reflecting reduced responsiveness of beta cells to glucose stimulation and reduced responsiveness of peripheral tissues to insulin^{18–20}. Beta cell proliferation declines dramatically at an early age, potentially contributing to a reduced beta cell mass and an increased risk of diabetes with age²¹. Expression of p16 increases in beta cells during aging, inhibiting their regenerative capacity^{9,22}. Genetic polymorphisms in the *CDKN2A* locus are associated with type 2 diabetes²³; however, their functional consequences are unknown. Components of the cell cycle machinery, including CDK4, RB1 and the E2F family of transcription factors, have been implicated in various aspects of glucose homeostasis, including short-term responses to glucose stimulation by beta cells and responses to insulin by peripheral tissues^{24–28}. However, it is unknown whether the age-associated elevation of p16 expression in beta cells leads to cellular senescence and whether such cells remain functional. Here we report that increased p16 activity enhances insulin secretion by beta cells upon glucose stimulation. We found that

¹Department of Developmental Biology and Cancer Research, Institute for Medical Research—Israel-Canada, Hebrew University—Hadassah Medical School, Jerusalem, Israel. ²Computation Center, Hebrew University—Hadassah Medical School, Jerusalem, Israel. ³Endocrinology and Metabolism Service, Department of Internal Medicine, Hadassah-Hebrew University Medical Center, Jerusalem, Israel. ⁴Division of Diabetes, Endocrinology and Metabolism, Department of Medicine, Vanderbilt University Medical Center, Nashville, Tennessee, USA. ⁵Department of Molecular Physiology and Biophysics, Vanderbilt University School of Medicine, Nashville, Tennessee, USA. ⁶Veteran Affairs Tennessee Valley Healthcare System, Nashville, Tennessee, USA. ⁷Department of Surgery, University of Alberta, Edmonton, Alberta, Canada. ⁸Clinical Islet Transplant Program, University of Alberta, Edmonton, Alberta, Canada. ⁹Center for Stem Cell Biology, Vanderbilt University School of Medicine, Nashville, Tennessee, USA. Correspondence should be addressed to I.B.-P. (ittai@pmail.huji.ac.il) or Y.D. (yuvald@ekmd.huji.ac.il).

Received 17 December 2015; accepted 2 February 2016; published online 7 March 2016; doi:10.1038/nm.4054

p16 drives beta cell senescence during normal aging and that features of the senescence program—including increased cell size, elevated glucose uptake and mitochondrial activity—enhance the capacity of beta cells to secrete insulin after glucose stimulation.

RESULTS

p16 induces beta cell senescence

To study the effects of p16 expression on beta cell function, we generated mice that express the coding sequence for human p16 (which we refer to as *p16*) under the control of a tetracycline (tet)-inducible promoter (hereafter referred to as tet-p16 mice). We crossed these mice with *Ins2-rtTA* mice, in which the reverse tetracycline-controlled trans-activator protein (rtTA) is expressed from the promoter of the rat insulin 2 gene (*Ins2*). To activate p16 in beta cells, we treated double-transgenic *Ins2-rtTA*;tet-p16 mice with tet for 10 d starting at 3–4 weeks of age. Transgenic p16 was detected by immunostaining in ~35% of beta cells (Fig. 1a,b and Supplementary Fig. 1a). Staining for the cell proliferation marker Ki67 revealed that whereas 3.5% of beta cells in control (*Ins2-rtTA*) mice were proliferating, p16-expressing beta cells in the *Ins2-rtTA*;tet-p16 mice were nonproliferative (Fig. 1b,c). Senescence-associated β -galactosidase (SA- β -Gal) activity and expression of the lysosomal marker Lamp2a were increased in p16-expressing islets, indicating that p16 induces features of senescence (Fig. 1d,e). Notably, p16-expressing beta cells were ~1.3-fold larger than control beta

cells, as measured by both FACS and image analysis (Fig. 1f–h). Consistent with this, islets of p16-expressing mice had higher levels of phosphorylated ribosomal protein S6 (Rps6), a target of the mTOR protein and a regulator of beta cell size²⁹ (Fig. 1i and Supplementary Fig. 1b).

To isolate a population of beta cells enriched for p16 expression, we generated *Ins2-rtTA*;tet-p16;tet-GFP triple-transgenic mice, such that most of the p16⁺ cells would also express green fluorescent protein (GFP). We treated these and control *Ins2-rtTA*;tet-GFP mice with tet for 10 d, dissociated their islets and isolated GFP⁺ cells (Supplementary Fig. 1c). We compared the transcriptomes of p16-expressing and control GFP⁺ beta cells and found that gene sets associated with cell proliferation were downregulated in p16-expressing beta cells, whereas gene sets that were previously shown to be elevated in senescent cells were upregulated (Fig. 1j, Supplementary Fig. 2a,b and Supplementary Table 1). Notably, these latter sets were derived from diverse biological settings, including chemotherapy-treated lymphoma cells, *Ras* oncogene-expressing fibroblasts and fibrotic liver stellate cells^{15,30–33}. Genes encoding cytoskeletal proteins and some secreted proteins were also upregulated (Fig. 1j and Supplementary Table 1). mRNA levels of the p53 transcription factor target genes *Cdkn1a*, which encodes p21^{Cip1}, and *Serpine2*, which encodes Pai1, a marker of senescence, were higher in p16-expressing cells; however, expression of other target genes was not substantially induced, and p53 protein itself was not detected (Supplementary Fig. 2c–f).

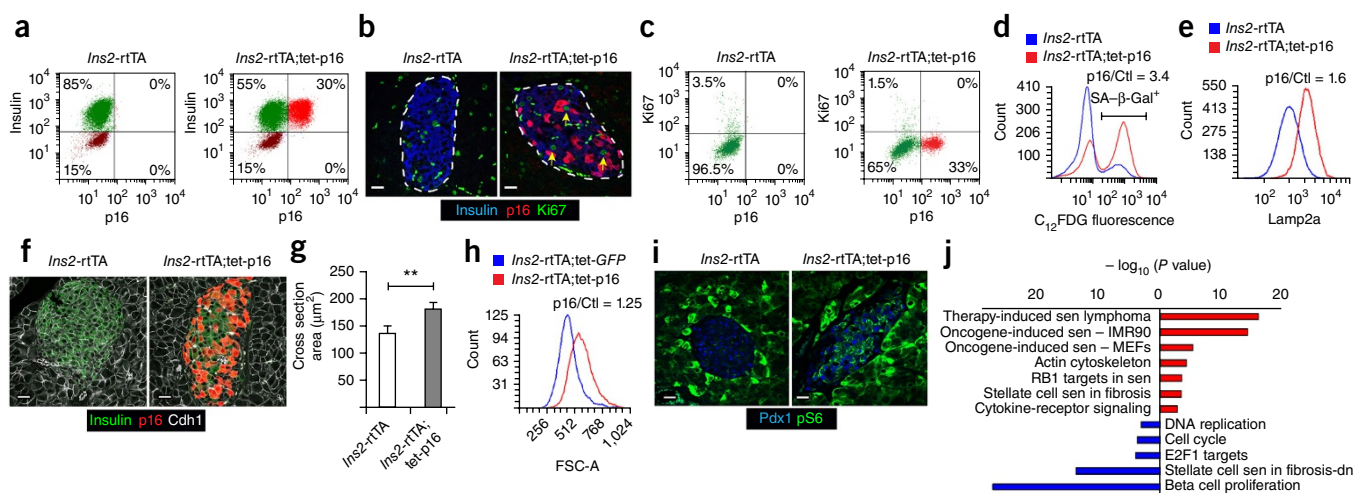


Figure 1 p16 induces senescence of beta cells. (a) FACS analysis of p16 and insulin expression in islet cells from control *Ins2-rtTA* (left) and *Ins2-rtTA*;tet-p16 (right) mice after tet treatment. The experiment was done ten times. (b) Representative images showing immunostaining of human p16 (red), the proliferation marker Ki67 (green) and insulin (to label beta cells; blue) in pancreatic islets (dotted line) of control *Ins2-rtTA* mice (left; of 12 images) and *Ins2-rtTA*;tet-p16 mice (right; of 21 images) ($n = 3$ mice per group). Arrows indicate Ki67⁺p16⁻ cells. (c) FACS analysis of p16 and Ki67 expression in insulin⁺ cells from dissociated islets of control *Ins2-rtTA* (left) and *Ins2-rtTA*;tet-p16 (right) mice. The experiment was repeated three times. (d) FACS analysis of SA- β -Gal activity (as measured by the fluorescent β -Gal substrate C₁₂FDG) in islet cells from the indicated mice. The ratio of SA- β -Gal⁺ cells in p16-expressing versus control mice (p16/Ctl) is indicated. The experiment was done twice. (e) FACS analysis of the expression of the lysosomal protein Lamp2a in insulin⁺ cells from the indicated mice. Red line shows p16⁺ cells. (f) Representative images of islets from the indicated mice that were stained, for the purpose of measurement of beta cell size, for human p16 (red), insulin (green) and E-cadherin (Cdh1, white). (g) Quantification of the cross-sectional areas of beta cells from control *Ins2-rtTA* mice (left) and of p16⁺ beta cells from *Ins2-rtTA*;tet-p16 mice (right), done by image analysis of sections stained as in f ($n = 6$ mice per group; >100 cells were measured in each mouse). Data are mean \pm s.d. ** $P < 0.005$; by Student's *t*-test. (h) Forward scatter (FSC-A) histograms of insulin⁺ cells from the indicated mice. Red line shows p16⁺ cells. The experiment was repeated five times. (i) Representative images showing Pdx1 (blue) and phospho-S6 (pS6, green) expression in islets from control *Ins2-rtTA* (left; of 12 images) and *Ins2-rtTA*;tet-p16 (right; of 24 images) ($n = 3$ mice per group). (j) Enrichment significance of gene sets associated with senescence (sen) and proliferation (top graph), or with beta cell maturation and differentiation (bottom graph), among genes upregulated (red) or downregulated (blue) in p16-expressing beta cells. Values indicate $-\log_{10}(P \text{ value})$; by hypergeometric test. MEFs, mouse embryo fibroblasts; IMR90, normal human fibroblasts; fibrosis-dn, genes downregulated in senescent stellate cells. Throughout, scale bars, 20 μm .

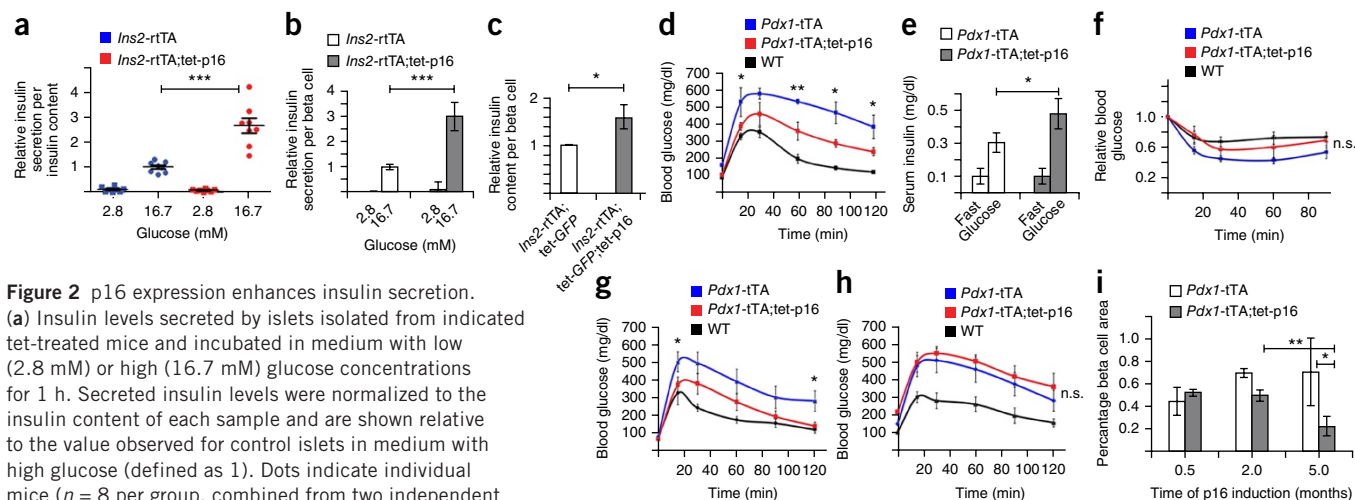


Figure 2 p16 expression enhances insulin secretion. (a) Insulin levels secreted by islets isolated from indicated tet-treated mice and incubated in medium with low (2.8 mM) or high (16.7 mM) glucose concentrations for 1 h. Secreted insulin levels were normalized to the insulin content of each sample and are shown relative to the value observed for control islets in medium with high glucose (defined as 1). Dots indicate individual mice ($n = 8$ per group, combined from two independent experiments), and each shows the mean of three replicates per mouse. The experiment was done four times. (b) Mean insulin levels secreted by islets from the indicated mice and assayed as in a. Secreted insulin levels were normalized to beta cell number in each sample and are shown relative to the value observed for control islets in medium with high glucose (defined as 1). Islets were pooled from three mice and assayed in five replicates per group. (c) Insulin content in equal numbers of beta cells, sorted on the basis of GFP expression, from control (*Ins2-rtTA*;tet-*GFP*) or p16-expressing (*Ins2-rtTA*;tet-*GFP*;tet-*p16*) mice ($n = 2$ per group). Values are presented relative to those of the control. (d) Glucose tolerance test of wild-type (WT, $n = 2$), *Pdx1-tTA* ($n = 2$) and *Pdx1-tTA*;tet-*p16* ($n = 4$) mice following p16 activation for 2 weeks. The experiment was repeated in three independent mouse cohorts. (e) Serum insulin concentrations in the indicated mice after overnight fasting (fast) or 10 min after glucose injection (glucose) ($n = 3$ mice per group). (f) Insulin tolerance test in the indicated mice following p16 activation for 10 d ($n = 3$ mice per group). (g,h) Glucose tolerance test of WT ($n = 3$), *Pdx1-tTA* ($n = 4$) and *Pdx1-tTA*;tet-*p16* ($n = 6$) mice following p16 activation for 2 (g) or 5 (h) months. (i) Percentage of insulin⁺ area in pancreatic sections of the indicated mice at 2 weeks, 2 months or 5 months after p16 activation ($n = 3$ mice per group). Error bars indicate s.e.m. in all panels, except in b (in which they indicate s.d.). Throughout, * $P < 0.05$, ** $P < 0.005$, *** $P < 0.0005$; n.s., not significant; by Student's *t*-test.

Thus, p16 expression is sufficient to activate hallmarks of the senescence gene-expression program in beta cells.

Key markers and regulators of beta cell differentiation were minimally changed after p16 expression (Supplementary Fig. 3a–d), indicating that the cells maintained their identity. However, we observed upregulation of genes whose expression increases in adult versus neonatal beta cells concomitant with the acquisition of functionality³⁴ (Fig. 1j and Supplementary Fig. 3e). Polycomb repressive complex target genes (i.e., genes bound by trimethylated lysine 27 of histone H3 (H3K27me3) in embryonic stem cells) were upregulated, as were additional sets associated with beta cell differentiation and aging^{22,35} (Fig. 1j and Supplementary Fig. 3f). These findings suggested that p16 and senescence enhance aspects of beta cell maturation.

p16 increases glucose-stimulated insulin secretion

To directly study the effect of p16 expression on beta cell function, we isolated pancreatic islets from p16-expressing and control mice after 10 d of tet treatment and measured GSIS. Islets from the two groups of mice secreted similar levels of insulin after incubation in medium with low concentrations of glucose; however, after glucose stimulation, p16-expressing islets secreted ~2.5-fold more insulin than control islets (Fig. 2a).

This difference was evident when the insulin concentrations were normalized to total insulin and protein content in the islet samples, or to beta cell numbers (Fig. 2a,b and Supplementary Fig. 4a). High GSIS was also observed after p16 induction in sexually mature mice (Supplementary Fig. 4b), as well as after 2 months of p16 induction, indicating a stable phenotypic change in beta cell function (Supplementary Fig. 4c). Furthermore, we found that p16-expressing beta cells had ~1.5-fold higher intracellular insulin content than control beta cells (Fig. 2c). Thus, p16 expression increases the capacity of beta cells to release insulin following glucose stimulation.

p16 induction improves glucose tolerance in mice with diabetes

Improved beta cell function could be expected to alter physiological glucose tolerance. *Ins2-rtTA*;tet-*p16* mice were, however, not suitable for testing this hypothesis, as they suffered from decreased overall beta cell mass owing to low tet-independent p16 expression (Supplementary Fig. 4d–g). We therefore tested the effects of p16 induction in *Pdx1-tTA* mice, in which the tet transactivator protein (tTA) is expressed from the gene encoding the pancreatic and duodenal homeobox 1 transcription factor (*Pdx1*). These mice are deficient in one allele of the *Pdx1* gene, mimicking a monogenic familial form of diabetes, maturity-onset diabetes of the young (MODY) 4 (refs. 36,37). Because the hyperglycemia in these mice is caused by impaired beta cell function rather than by systemic abnormalities, they were particularly suitable for this analysis³⁷. Furthermore, the *Pdx1-tTA* transgene allowed tightly regulated beta cell-specific activation of the tet-*p16* transgene (Supplementary Fig. 5a).

We induced p16 expression in 1-month-old *Pdx1-tTA*;tet-*p16* mice for 2 weeks. Glucose tolerance was improved in these mice as compared to the hyperglycemic *Pdx1-tTA* mice, indicating that p16 expression partially reverses the impaired function of beta cells (Fig. 2d). Serum insulin levels following glucose injection were higher in *Pdx1-tTA*;tet-*p16* mice than in *Pdx1-tTA* mice, accounting for their improved glucose tolerance (Fig. 2e). Beta cells of p16-expressing mice were larger than those of *Pdx1-tTA* mice, which were smaller than those of wild-type (WT) mice (Supplementary Fig. 5b). Sensitivity to insulin and body mass were not significantly affected by p16 expression (Fig. 2f and Supplementary Fig. 5c), consistent with the conclusion that increased insulin secretion by beta cells was the primary cause of improved glucose tolerance.

After 2 months of p16 induction, *Pdx1-tTA*;tet-*p16* mice still showed improved glucose tolerance (Fig. 2g); however, after 5 months of induction their glucose tolerance deteriorated to levels observed

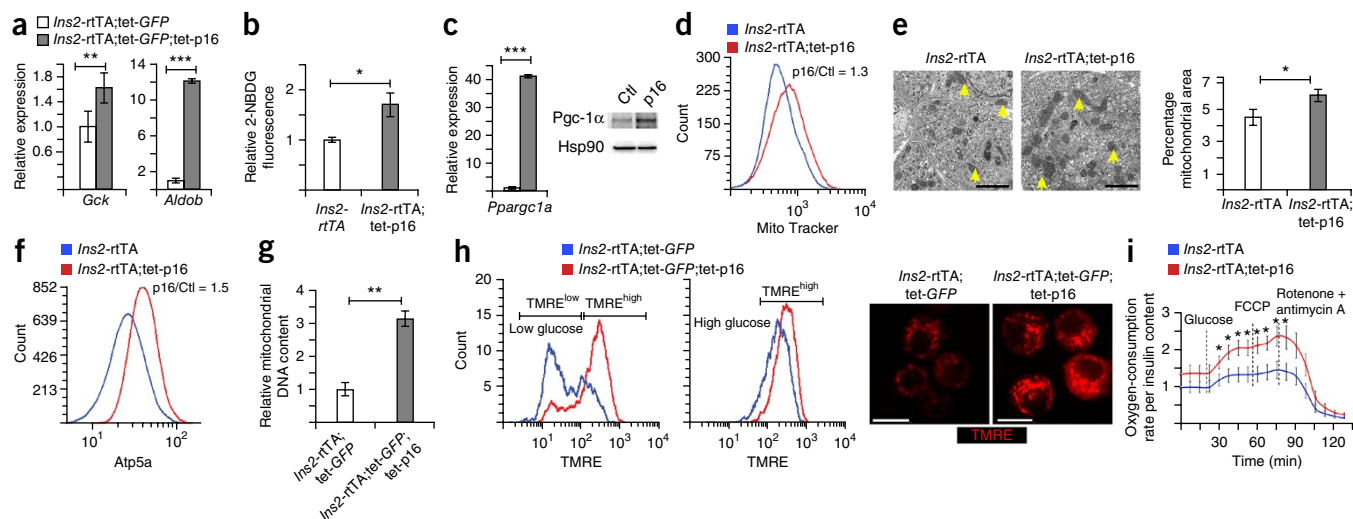


Figure 3 p16 expression increases glucose uptake and mitochondrial activity. **(a)** Relative mRNA levels of *Gck* and *Aldob* in GFP⁺ beta cells of control *Ins2-rtTA*;tet-*GFP* ($n = 2$) and p16-expressing *Ins2-rtTA*;tet-*GFP*;tet-p16 ($n = 3$) mice. Error bars indicate s.e.m. **(b)** Relative glucose uptake rates in dissociated islet cells from the indicated mice, as measured by FACS analysis after incubation with the fluorescent glucose analog 2-NBDG for 30 min. Values are mean \pm s.e.m. of five samples, each comprised of cells from three mice. **(c)** Relative mRNA levels of *Ppargc1a* in mice (indicated as in panel **a**) (left) and western blot of Pgc-1 α in control and p16-expressing islets (right; done twice). Hsp90 is shown as a loading control. Error bars indicate s.e.m. **(d)** FACS analysis of islet cells from the indicated mice that were stained with MitoTracker to label mitochondria. p16/Ctl indicates the ratio of the mean fluorescence value from p16-expressing cells to that from control cells. **(e)** Representative electron microscopy images of beta cells from control *Ins2-rtTA* (left) and *Ins2-rtTA*;tet-p16 (middle) mice. Right, quantification of the mitochondrial area as a percentage of the analyzed images. Values indicate mean (\pm s.e.m.) of control cells ($n = 20$) and cells from p16-expressing islets ($n = 23$), obtained from a total of five mice per group. Yellow arrows indicate mitochondria. Scale bars, 2 μ m. **(f)** FACS analysis of expression of the mitochondrial protein Atp5a in insulin⁺ islet cells from the indicated mice. Red line shows p16⁺ cells. The experiment was done once. **(g)** Mitochondrial DNA content, as measured by qPCR of the mitochondrial cytochrome *b* gene (*mt-Cytb*), in DNA extracted from equal numbers of GFP⁺ cells pooled from five mice per indicated group. Values were normalized to the levels of the L1 genomic repeat sequence and are presented as a mean of triplicate reactions \pm s.e.m. **(h)** Left, FACS analyses of GFP⁺ cells isolated and pooled from five mice per group after incubation in medium with low (3 mM) or high (20 mM) concentrations of glucose (as indicated) and stained with the mitochondrial membrane potential indicator dye TMRE. Right, representative images of cells stained with TMRE after incubation in high-glucose medium as measured by FACS. The FACS experiment was repeated three times. Scale bars, 10 μ m. **(i)** Oxygen-consumption rates of islets isolated from the indicated mice. Glucose (20 mM), the membrane uncoupler FCCP, and the electron transport chain inhibitors rotenone + antimycin A were added at the indicated times. Values were normalized to islet insulin content in each sample and are presented relative to the basal oxygen-consumption levels of control islets (defined as 1). Data are mean \pm s.e.m. of five replicates, each containing 40 islets pooled from five mice. The experiment was repeated three times. Throughout, * $P < 0.05$, ** $P < 0.005$, *** $P < 0.0005$; by Student's *t*-test.

in *Pdx1*-tTA mice (Fig. 2h). At this time point, beta cell mass was substantially lower in these mice, presumably due to reduced beta cell proliferation, and this could account for the decline in glucose tolerance (Fig. 2i and Supplementary Fig. 5d).

p16 enhances glucose uptake and mitochondrial activity

Insulin secretion is primarily controlled by oxidative metabolism of glucose in the mitochondria, resulting in increased cellular ATP levels, which in turn causes membrane depolarization, calcium influx and insulin release³⁸. Recent studies have shown that senescence involves enhanced glucose uptake and metabolism^{14–17}. We found that p16-expressing beta cells upregulated genes associated with glucose metabolism (Fig. 1j), including *Aldob*, which encodes the glycolytic enzyme fructose-bisphosphate aldolase B, and *Gck*, which encodes glucokinase, the enzyme that controls glucose uptake and glycolysis rates (Fig. 3a). Consistent with this, the glucose uptake rate in cells isolated from p16-expressing islets was 1.7-fold higher than that in cells isolated from control islets (Fig. 3b).

The levels of peroxisome proliferative-activated receptor gamma coactivator 1 alpha (*Ppargc1a*; hereafter referred to as Pgc-1 α)—the master transcription factor controlling mitochondrial biogenesis—were higher in p16-expressing beta cells than in controls (Fig. 3c). We found that, indeed, p16-expressing beta cells contained higher numbers of mitochondria, as assessed by electron microscopy, stains

of mitochondrial markers and quantification of mitochondrial DNA content (Fig. 3d–g). Furthermore, mitochondrial membrane potential, an indicator of mitochondrial activity, was higher in p16-expressing beta cells (Fig. 3h). p16-expressing islets consumed more oxygen in basal conditions and in response to glucose stimulation than control islets (Fig. 3i). Thus, p16 expression in beta cells leads to elevated levels of glucose uptake, mitochondrial biogenesis and mitochondrial respiration, providing a link to higher GSIS.

Endogenous p16 drives an increase in GSIS capacity with age

We next asked whether endogenous p16, whose expression increases in beta cells with age⁹, influences insulin secretion. Islets isolated from WT mice at 6, 11 and 27 months of age showed higher GSIS than islets of 1-month-old (juvenile) mice, concomitant with their higher p16 levels (Fig. 4a,b). Beta cells of the more mature mice had lower proliferation rates, were larger and had higher SA- β -Gal activity (Fig. 4c,d and Supplementary Fig. 6a). Notably, unlike p16-overexpressing transgenic mice, islets of mature WT mice showed higher insulin secretion than those of juvenile mice also at low concentrations of glucose; the fold change in insulin secretion between high and low glucose concentrations was therefore unchanged during aging (Fig. 4a and Supplementary Fig. 6b,c).

To study whether p16 contributes to the higher GSIS observed in mature mice, we examined the pancreata of p16-deficient mice.

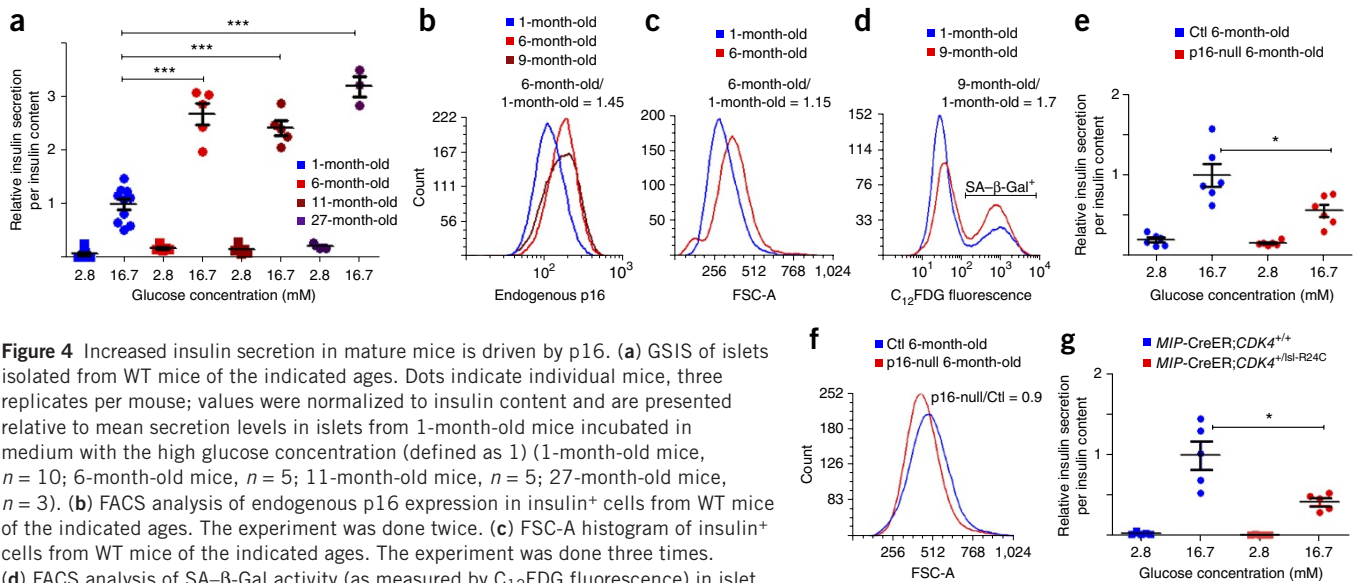


Figure 4 Increased insulin secretion in mature mice is driven by p16. **(a)** GSIS of islets isolated from WT mice of the indicated ages. Dots indicate individual mice, three replicates per mouse; values were normalized to insulin content and are presented relative to mean secretion levels in islets from 1-month-old mice incubated in medium with the high glucose concentration (defined as 1) (1-month-old mice, $n = 10$; 6-month-old mice, $n = 5$; 11-month-old mice, $n = 5$; 27-month-old mice, $n = 3$). **(b)** FACS analysis of endogenous p16 expression in insulin⁺ cells from WT mice of the indicated ages. The experiment was done twice. **(c)** FSC-A histogram of insulin⁺ cells from WT mice of the indicated ages. The experiment was done three times. **(d)** FACS analysis of SA-β-Gal activity (as measured by C₁₂FDG fluorescence) in islet cells from WT mice of the indicated ages. The experiment was done twice. **(e)** GSIS of islets from 6-month-old WT and p16-deficient mice ($n = 6$ per group). Values were normalized to insulin content and are presented relative to the secretion level of control islets incubated in medium with high glucose (defined as 1). **(f)** FSC-A histogram of insulin⁺ cells from 6-month-old control and p16-deficient mice. The experiment was done twice. p16-null/Ctl indicates the ratio of the mean fluorescence value from p16-deficient cells to that from the control cells. **(g)** GSIS of islets from 2-month-old *MIP-CreER;CDK4^{+/Isl-R24C}* and control *MIP-CreER;CDK4^{+/+}* mice 2 weeks after Cre activation ($n = 5$ per group). Values were normalized to insulin content and are presented relative to the secretion level of control islets incubated in medium with high glucose (defined as 1). Throughout, error bars indicate mean \pm s.e.m. * $P < 0.05$, *** $P < 0.0005$; by Student's *t*-test.

As previously reported⁹, the number of proliferating beta cells was approximately twofold higher in 6- and 12-month-old p16-deficient mice than in WT control mice (**Supplementary Fig. 6a**). However, GSIS of islets from mature p16-deficient mice was lower than that of control mouse islets, and the beta cells from these p16-deficient mice were smaller (**Fig. 4e,f**), indicating that endogenous p16 promotes increased beta cell size and GSIS with age.

The main function of p16 is the inhibition of CDK4 (ref. 5). We therefore tested whether expression of a constitutively active CDK4 would mimic the effect of p16 deficiency and reduce GSIS. To do this we crossed mice carrying a conditional knocked-in mutated *CDK4^{R24C}* allele (*CDK4^{+/Isl-R24C}* mice)³⁹ with mice expressing a tamoxifen-inducible *Cre* under the control of the mouse insulin promoter (*MIP-CreER*)⁴⁰ (**Supplementary Fig. 6d**). We activated the translation of the *CDK4^{R24C}* protein in beta cells by tamoxifen injection and collected islets 2 weeks later. Islets from *MIP-CreER;CDK4^{+/R24C}* mice showed lower GSIS than those of control mice, recapitulating the effects of p16 deficiency (**Fig. 4g**). This finding supports the hypothesis that p16 enhances GSIS through CDK4 inhibition.

Beta cell senescence in human islets

We next tested whether beta cell senescence occurs in humans. Immunostaining of human islets revealed that p16 expression was higher in aged subjects than in young subjects, and that p16 mRNA levels were similarly elevated with age (**Fig. 5a,b** and **Supplementary Table 2**). We dissociated live human islets obtained from recently deceased middle-aged human subjects and co-stained the cells for p16 and insulin (**Fig. 5c** and **Supplementary Fig. 1**). This analysis identified a subset of p16⁺ beta cells, and these cells had a larger mean volume than p16⁻ beta cells from the same islets (**Fig. 5c,d**). As in p16-expressing transgenic mice, levels of phosphorylated S6 were higher in aged versus young subjects (**Fig. 5e** and **Supplementary Fig. 7a**).

Live, dissociated human islets obtained from middle-aged donors contained a substantial fraction of SA-β-Gal⁺ cells (range 40–60% of cells; mean \pm s.d., 50% \pm 8% cells; $n = 5$) (**Fig. 5f** and **Supplementary Table 3**). We obtained one sample from a young (14-year-old) subject, which did not contain SA-β-Gal⁺ cells (**Fig. 5f**). SA-β-Gal⁺ cells from adult islets contained more active mitochondria than SA-β-Gal⁻ cells from the same islets (**Fig. 5g**). In addition, sections of pancreas from middle-aged subjects showed higher levels of mitochondrial proteins than those from young subjects (**Fig. 5h** and **Supplementary Fig. 7b**). Together, these findings indicate that during human aging p16-expressing senescent beta cells accumulate in islets and that these cells are larger in size and have increased mitochondrial numbers and activity.

p16-induced senescence of human cells increases GSIS

We next tested whether senescence of human cells leads to increased insulin secretion. EndoC-βH2 cells are a line of human fetal pancreas-derived insulin-expressing cells that was propagated by introduction of the SV40 large T antigen and the human telomerase reverse transcriptase (*TERT*) genes⁴¹. Cre-mediated excision of these immortalizing genes re-activates RB1 and p53, causing the cells to cease dividing and to increase insulin expression and secretion⁴¹. We found that EndoC-βH2 cells infected with a *Cre*-expressing lentivirus acquired a senescent morphology and had high levels of SA-β-Gal activity, consistent with the known roles of RB1 and p53 in senescence induction (**Fig. 6a,b**). This was accompanied by a substantial elevation in insulin secretion (**Fig. 6c,d**). Senescent EndoC-βH2 cells were larger, and had higher glucose uptake and mitochondrial activity, than control cells (**Fig. 6e**).

EndoC-βH2 cells expressed the endogenous p16, and its expression level was further elevated after the introduction of *Cre* (**Supplementary Fig. 8a,b**). To test whether p16 drives senescence and enhanced GSIS in the EndoC-βH2 cells, we generated cells in

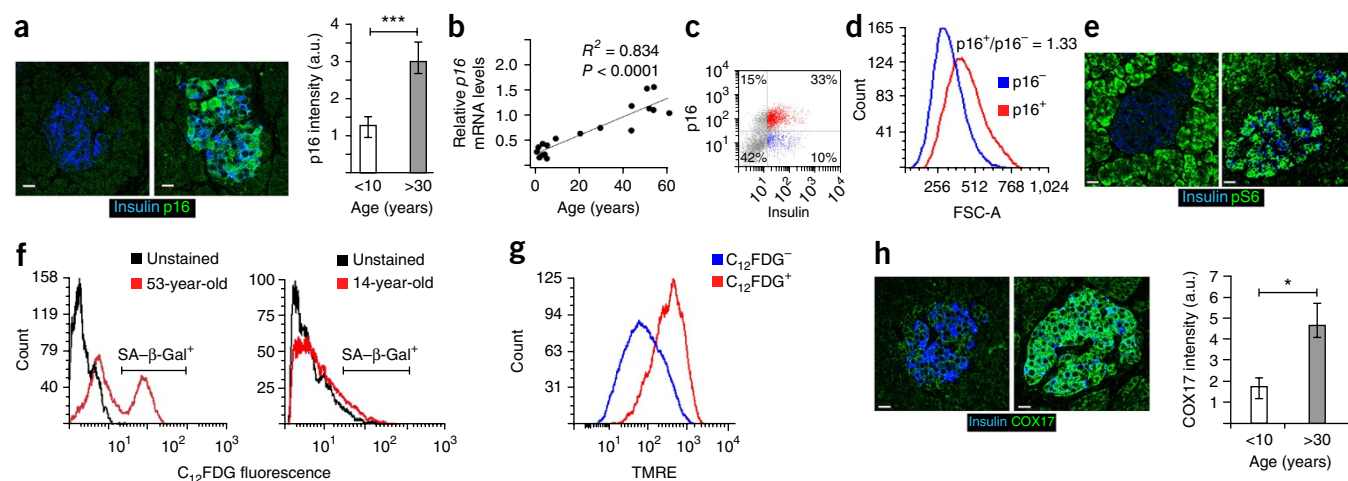


Figure 5 Senescent beta cells in human islets. **(a)** Representative islet sections of juvenile (left; 5-month-old) and adult (middle; 45-year-old) human subjects stained for insulin (blue) and p16 (green), and quantification of the mean intensity of p16 staining in juvenile subjects (5-month-old to 10-year-old; $n = 6$; 46 sections stained) and adult subjects (30- to 60-year-old; $n = 5$; 40 sections stained) (right). a.u., arbitrary units. **(b)** Relative *p16* mRNA levels in islets from human subjects aged 6 months to 60 years ($n = 18$). **(c)** FACS analysis of dissociated islets from a 42-year-old subject stained for insulin and p16. Red dots indicate insulin+p16⁺ cells. The experiment was done three times. **(d)** FSC-A histograms of insulin+p16⁻ and insulin+p16⁺ cells within islets of a 56-year-old subject. The experiment was done three times. **(e)** Representative islet sections of juvenile (left; 5-month-old) and adult (right; 51-year-old) human subjects stained for insulin (blue) and pS6 (green). Subjects as in **a**; 61 islet sections from juvenile and 51 sections from adult human subjects were stained. **(f)** SA-β-Gal activity (measured by C₁₂FDG fluorescence) in live islet cells from a 53-year-old (left) and a 14-year-old (right) human subject. Five adults and one young subject were analyzed (see **Supplementary Table 3**). **(g)** FACS analysis of TMRE-stained SA-β-Gal⁺ and SA-β-Gal⁻ islet cells isolated from a 53-year-old human subject. The experiment was repeated three times. **(h)** Representative islet sections from a 5-year-old (left) and a 45-year-old (middle) human subject stained for insulin (blue) and the mitochondrial protein COX17 (green), and quantification of mean COX17 intensity in sections from subjects as in **a** (juvenile, $n = 46$ sections; adult, $n = 46$ sections) (right). Throughout, error bars indicate s.e.m. * $P < 0.05$, *** $P < 0.0005$; by Student's *t*-test. Scale bars, 20 μm.

which p16 expression was stably silenced by a short hairpin RNA targeting the *p16* transcript (shp16). We then infected these cells with a *Cre*-expressing virus to activate RB1 and p53. We found that although *p16*-silenced cells stopped dividing after *Cre* expression, they showed substantially lower levels of SA-β-Gal activity than *p16*-expressing cells (**Fig. 6f** and **Supplementary Fig. 8c,d**). Notably, the *p16*-silenced cells did not show increased GSIS capacity or increased mitochondrial activity after *Cre* expression (**Fig. 6g,h**). These findings indicate that endogenous p16 expression is necessary for the entry of these human cells into senescence and for the acquisition of enhanced GSIS.

mTOR and PPAR-γ contribute to enhanced GSIS in senescent cells

Given the known roles of mTOR in regulating beta cell size and mitochondrial biogenesis and function^{29,42–44}, we tested the effects of its inhibition on EndoC-βH2 cells undergoing senescence. Cells treated with the kinase inhibitor Torin1 after introduction of *Cre* had lower levels of insulin secretion, as well as reduced size and mitochondrial activity, than untreated cells (**Fig. 6i** and **Supplementary Fig. 8e,f**).

Inhibition of PPAR-γ, the binding partner of PGC-1α, by treatment with GW9662 also resulted in lower GSIS and mitochondrial activity in *Cre*-expressing EndoC-βH2 cells (**Fig. 6i** and **Supplementary Fig. 8g**). The activities of mTOR and PPAR-γ thus contribute to increased GSIS during senescence (**Fig. 6j**).

DISCUSSION

p16 expression increases in human and mouse beta cells with age, and previous work showed that this contributes to their reduction in regenerative capacity^{9,22}. Our findings indicate that p16 concomitantly improves the primary function of beta cells, glucose-stimulated insulin secretion (**Fig. 6j**). We find that GSIS increases during normal aging of mice and that this functional improvement is driven

by p16. This provides a novel view of beta cell maturation during healthy aging that includes functional enhancement. In the setting of hyperglycemia, p16 expression provided a substantial physiologic benefit within days, which was stably maintained. Our observations of increased p16 expression and senescence in human islets, and our experiments in human cells, strongly suggest that senescence-induced enhancement of GSIS is conserved between mice and humans, and point to p16 as its main driver in both organisms.

Beta cell proliferative capacity and functionality appear to be at mutual expense. Because adult beta cells rarely proliferate, the functional benefit of p16 activity may be prominent at early stages of its expression. However, after prolonged periods of p16 expression beta cell mass may diminish owing to loss of self-duplication⁴⁵, and this could lead to deficient glucose tolerance with age. This is illustrated by the deterioration in glucose tolerance that we observed in *Pdx1-tTA;tet-p16* mice after 5 months of p16 induction.

Measurement of beta cell function *in vivo* is challenging because of the complex dynamics of insulin release and uptake, the responses of peripheral tissues and the systemic changes in glucose levels. Insulin secretion is often measured as the fold change between fasting and glucose-stimulated states, and this parameter is generally reduced with age, consistent with overall reduced glucose tolerance^{18–20}. However, in human subjects, both basal and stimulated insulin secretion levels have been documented to increase with age¹⁸, and we observed the same phenomenon in mice. A recent study in which beta cell function was monitored in thousands of subjects over a 10-year period revealed that insulin secretion does indeed rise with age in healthy subjects⁴⁶.

We established the enhancement of GSIS by p16 in *ex vivo* experiments, in which systemic effects are absent, as well as *in vivo*, in the context of hyperglycemia. Notably, p16 overexpression or loss of

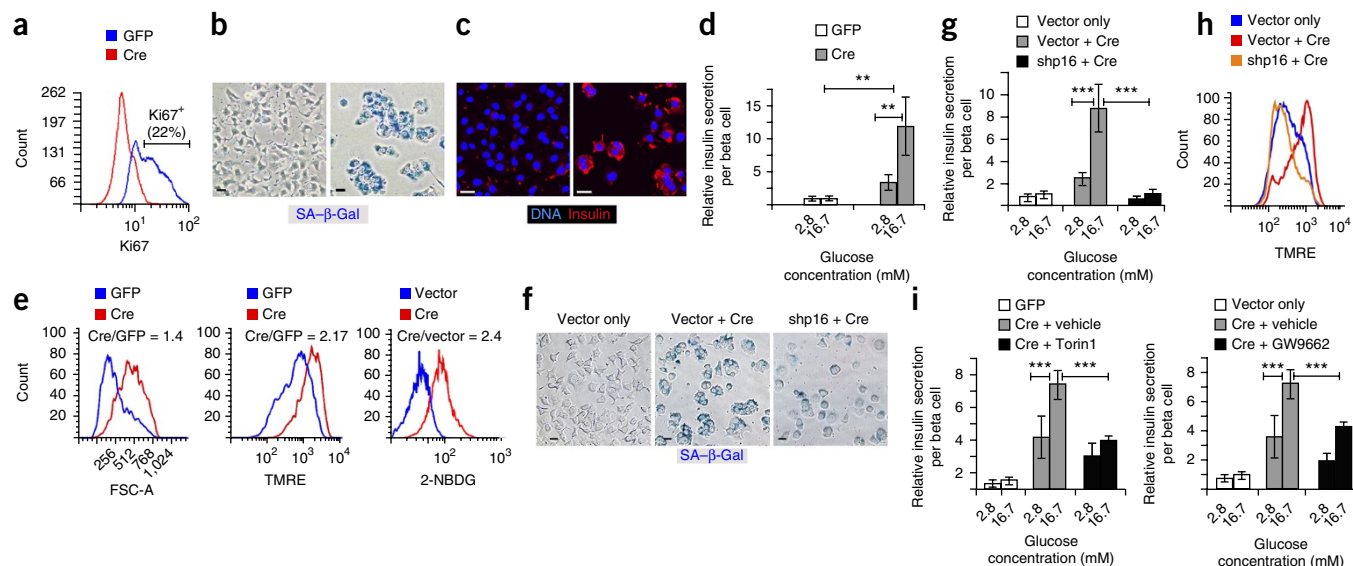


Figure 6 p16-induced senescence of human cells leads to enhanced GSIS. **(a)** FACS analysis of Ki67-stained EndoC-βH2 cells 3 weeks after infection with a lentivirus expressing *GFP* (blue line) or *Cre + GFP* (red line); *GFP*⁺ cells are shown. The experiment was done three times. **(b)** Representative images (out of ten taken) of EndoC-βH2 cells expressing *GFP* (left) or *Cre + GFP* (right) stained for SA-β-Gal activity (blue) in 3 weeks after infection. **(c)** Representative images (out of ten taken) of EndoC-βH2 cells expressing either *GFP* (left) or *Cre + GFP* (right) that were stained for insulin (red). **(d)** Insulin secretion levels by EndoC-βH2 cells expressing either *GFP* (white) or *Cre + GFP* (gray) after incubation in medium containing low (2.8 mM) or high (16.7 mM) glucose concentrations for 1 h. Values are the mean of four replicates per group \pm s.d., normalized to cell number and shown relative to insulin levels in control cells incubated in medium with high glucose (defined as 1). **(e)** FACS analyses of FSC-A, TMRE staining and 2-NBDG fluorescence in control and *Cre*-expressing cells. The ratios indicate the mean fluorescence value from *Cre*-expressing to that from control cells. **(f)** Representative images (out of ten taken) of SA-β-Gal activity (blue) in EndoC-βH2 cells infected with an empty vector alone (left), an empty vector followed by the *Cre*-expressing lentivirus (middle) or an shp16-expressing construct followed by the *Cre*-expressing lentivirus (right). **(g)** Insulin secretion levels by EndoC-βH2 cells infected with an empty vector alone, an empty vector followed by the *Cre*-expressing lentivirus or an shp16-expressing construct followed by the *Cre*-expressing lentivirus (black), analyzed as in **d**. Values are the mean of five replicates \pm s.d. **(h)** FACS analysis of TMRE staining in the cells indicated in **g**. **(i)** Left, insulin secretion levels by control (*GFP* only) and *Cre*-expressing cells treated with vehicle or the mTOR inhibitor Torin1 for 3 weeks. Right, similar analysis of control (vector only) and *Cre*-expressing cells treated with either vehicle or the PPAR-γ inhibitor GW9662 for 3 weeks. Values are the mean of five replicates \pm s.d. **(j)** Schematic diagram summarizing the effects of p16-induced senescence on beta cell function. Components of the senescence program that contribute to increased insulin secretion are highlighted in red. Question mark represents potential additional effectors. Throughout, ** $P < 0.005$, *** $P < 0.0005$; by Student's *t*-test. Scale bars, 20 μm.

function affected insulin secretion at high, but not low, glucose levels. p16 thus appears to control this particular component of the age-associated changes in beta cell function, whereas additional factors may affect other parameters that contribute to the overall deterioration of beta cell function and glucose homeostasis.

Activation of RB1 through CDK4 inhibition is the central well-established function of p16, and RB1 is the main regulator of the chromatin reprogramming that leads to senescence^{5,30,47–49}. Our findings indeed suggest that p16 induces beta cell senescence and enhanced GSIS through CDK4 and RB1. CDK4 overactivation in mouse beta cells reduced GSIS, mimicking p16 deficiency, whereas in human cells, high endogenous p16 levels induced senescence and GSIS only after RB1 and p53 were released from inhibition by the SV40 large T antigen. However, the specific downstream components that are most important in mediating the senescence-associated increase in GSIS remain to be elucidated.

Senescence involves a coordinated reprogramming of cell structure and function. Multiple parameters indicate that the senescence program was activated in p16-expressing beta cells, including the induction of SA-β-Gal activity, the expression of markers such as

Lamp2a and *SerpinE2* and the upregulation of multiple senescence-associated gene sets. Inherent features of the senescence program appear to have been co-opted in beta cells to enhance insulin secretion (**Fig. 6j**). This provides an example of senescence having a role in enhancing normal cellular functionality, rather than leading to cell dysfunction. Enlarged cell size is a hallmark of senescence, which, to date, has been described mostly in cultured cells; p16 expression and senescence consistently increased beta cell size, a feature associated with increased secretory capacity^{29,50}. The inhibition of EndoC-βH2 cell enlargement by treatment with Torin1 indicates that this feature is mediated in part by mTOR.

Increased glucose uptake, oxidative phosphorylation and mitochondrial biogenesis have recently been highlighted as key features of senescence and are driven, at least in some cases, by RB1 (refs. 15–17,51,52). These metabolic changes, which we showed to occur in senescent mouse beta cells and human cells, provide a mechanistic link to insulin secretion, which is directly regulated by ATP levels³⁸. Our findings indicate that mTOR and PPAR-γ, the latter potentially functioning together with PGC-1α, contribute to the increased mitochondrial activity observed in senescence.

Genes associated with the functional maturation of beta cells were upregulated in p16-expressing beta cells, suggesting that senescence leads to enhanced differentiation of these cells, potentially through reduced activity of Polycomb. This is consistent with recent work suggesting that aging-associated changes in chromatin structure increase beta cell maturation and function⁵³.

The finding that senescence regulates insulin secretion has broad implications for the understanding and treatment of diseases involving beta cell malfunction and highlights the potential effects of drugs that target senescence and the cell cycle on beta cell function. PPAR- γ agonists are well-described therapies for type 2 diabetes that influence peripheral-tissue responses to insulin⁵⁴; our findings demonstrate the potential importance of this pathway to beta cell function during aging. Additionally, our findings raise the possibility that p16-expressing beta cells in aged subjects may show increased sensitivity to mTOR inhibition by a variety of drugs that are currently being evaluated in clinical trials.

Efforts to develop drugs that eliminate senescent cells from tissues for the potential treatment of aging-associated pathologies are ongoing^{2,55}. These are motivated, in part, by recent studies demonstrating that elimination of p16-expressing cells alleviates aging-associated tissue degeneration and extends mouse lifespan^{12,13}. In parallel, drugs that induce senescence are being developed, mainly for cancer treatment⁵⁶. Notable among the latter are inhibitors of CDK4 and CDK6, which in essence mimic p16 activity. The first of these was recently approved for breast cancer treatment⁵⁷. Our findings suggest that the potential effects of both classes of drugs on beta cell function should be taken into consideration and that the elimination of p16-expressing senescent beta cells may have negative effects on glucose homeostasis.

Overall, our findings highlight an important new aspect of senescence as a fundamental program that enhances cellular function during tissue maturation and aging. Although cumulative stress could potentially cause p16 activation and senescence in beta cells, our data suggest that p16 may, in fact, be activated as a component of the normal maturation of beta cells, executing a programmed developmental role not triggered by stress.

METHODS

Methods and any associated references are available in the [online version of the paper](#).

Accession codes. Gene Expression Omnibus: data are deposited under accession number [GSE76992](#).

Note: Any Supplementary Information and Source Data files are available in the online version of the paper.

ACKNOWLEDGMENTS

We thank M. Barbacid for *CDK4^{sl-R24C}* mice, L. Philipson for *MIP-CreER* mice, R. Scharfmann for the EndoC- β H2 cells; S. Efrat for the pTRIPAU3-CMV-nlsCre vector and C. Wright for the Pdx1-specific antibody. We thank N.E. Kidess-Bassir for histological preparation and T. Szoke for experimental assistance. This research was supported by a postdoctoral fellowship from the Juvenile Diabetes Research Foundation (A.H.) and by grants from Israel Science Foundation (grant no. 1009/13; I.B.-P.), the Jacob and Lena Joels Memorial Foundation Senior Lectureship for Excellence in the Life and Medical Sciences (I.B.-P.), Diabetes Onderzoek Nederland (Y.D. and I.B.-P.), the Alex U. Soyka program (Y.D. and I.B.-P.), the Juvenile Diabetes Research Foundation (Y.D. and A.C.P.), the US National Institutes of Health (NIH) Beta Cell Biology Consortium (Y.D.), the Leona M. and Harry B. Helmsley Charitable Trust (Y.D.), the Israeli Centers Of Research Excellence Program of the Planning and Budgeting Committee and the Israel Science Foundation (grant no. 41.11; Y.D.), the United States Agency for

International Development's American Schools and Hospitals Abroad Program (Y.D. and I.B.-P.), the Network for Pancreatic Organ Donors with Diabetes (nPOD) (Y.D.), the US Department of Veterans Affairs (A.C.P.), the National Institute of Diabetes and Digestive and Kidney Diseases–NIH (grant no. DK089572 (A.C.P.), DK72473 (A.C.P.) and DK104211 (A.C.P.)), and the Vanderbilt Diabetes Research and Training Center (grant no. DK20593; A.C.P.). Organ procurement organizations partnering with nPOD are listed at <http://www.jdrfnpod.org/our-partners.php>.

AUTHOR CONTRIBUTIONS

A.H., I.B.-P. and Y.D. designed experiments, analyzed data and wrote the manuscript; A.H. performed experiments; A.K., N.A., Y.G., E.H., S.A., A.S., R.C., Y.F., D.S., A.Z., S.T.-B., B.G., C.D. and A.C.P. did experiments and contributed experimental data; R.Z.G. and Y.N. performed bioinformatic analyses; A.M.J.S. contributed human islet samples; and M.A.M. assisted in generation of the tet-p16 mice.

COMPETING FINANCIAL INTERESTS

The authors declare competing financial interests: details are available in the [online version of the paper](#).

Reprints and permissions information is available online at <http://www.nature.com/reprints/index.html>.

- Muñoz-Espín, D. & Serrano, M. Cellular senescence: from physiology to pathology. *Nat. Rev. Mol. Cell Biol.* **15**, 482–496 (2014).
- van Deursen, J.M. The role of senescent cells in aging. *Nature* **509**, 439–446 (2014).
- Storer, M. *et al.* Senescence is a developmental mechanism that contributes to embryonic growth and patterning. *Cell* **155**, 1119–1130 (2013).
- Muñoz-Espín, D. *et al.* Programmed cell senescence during mammalian embryonic development. *Cell* **155**, 1104–1118 (2013).
- Kim, W.Y. & Sharpless, N.E. The regulation of INK4-Arf in cancer and aging. *Cell* **127**, 265–275 (2006).
- Nielsen, G.P. *et al.* Immunohistochemical survey of p16^{INK4A} expression in normal human adult and infant tissues. *Lab. Invest.* **79**, 1137–1143 (1999).
- Krishnamurthy, J. *et al.* Ink4a-Arf expression is a biomarker of aging. *J. Clin. Invest.* **114**, 1299–1307 (2004).
- Burd, C.E. *et al.* Monitoring tumorigenesis and senescence *in vivo* with a p16^{INK4a}-luciferase model. *Cell* **152**, 340–351 (2013).
- Krishnamurthy, J. *et al.* p16^{INK4a} induces an age-dependent decline in islet regenerative potential. *Nature* **443**, 453–457 (2006).
- Janzen, V. *et al.* Stem cell aging modified by the cyclin-dependent kinase inhibitor p16^{INK4a}. *Nature* **443**, 421–426 (2006).
- Molofsky, A.V. *et al.* Increasing p16^{INK4a} expression decreases forebrain progenitors and neurogenesis during aging. *Nature* **443**, 448–452 (2006).
- Baker, D.J. *et al.* Clearance of p16^{INK4a}-positive senescent cells delays aging-associated disorders. *Nature* **479**, 232–236 (2011).
- Baker, D.J. *et al.* Naturally occurring p16^{INK4a}-positive cells shorten healthy lifespan. *Nature* **530**, 184–189 (2015).
- Salama, R., Sadaie, M., Hoare, M. & Narita, M. Cellular senescence and its effector programs. *Genes Dev.* **28**, 99–114 (2014).
- Dörr, J.R. *et al.* Synthetic-lethal metabolic targeting of cellular senescence in cancer therapy. *Nature* **501**, 421–425 (2013).
- Kaplon, J. *et al.* A key role for mitochondrial gatekeeper pyruvate dehydrogenase in oncogene-induced senescence. *Nature* **498**, 109–112 (2013).
- Takebayashi, S. *et al.* Retinoblastoma protein promotes oxidative phosphorylation through upregulation of glycolytic genes in oncogene-induced senescent cells. *Aging Cell* **14**, 689–697 (2015).
- Gumbiner, B. *et al.* Effects of aging on insulin secretion. *Diabetes* **38**, 1549–1556 (1989).
- Iozzo, P. *et al.* Independent influence of age on basal insulin secretion in nondiabetic humans. *J. Clin. Endocrinol. Metab.* **84**, 863–868 (1999).
- Basu, R. *et al.* Mechanisms of the age-associated deterioration in glucose tolerance: contribution of alterations in insulin secretion, action and clearance. *Diabetes* **52**, 1738–1748 (2003).
- Kushner, J.A. The role of aging upon beta cell turnover. *J. Clin. Invest.* **123**, 990–995 (2013).
- Chen, H. *et al.* Polycomb protein Ezh2 regulates pancreatic beta cell Ink4a-Arf expression and regeneration in diabetes mellitus. *Genes Dev.* **23**, 975–985 (2009).
- Bao, X.Y., Xie, C. & Yang, M.S. Association between type 2 diabetes and CDKN2A/B: a meta-analysis study. *Mol. Biol. Rep.* **39**, 1609–1616 (2012).
- Annicotte, J.S. *et al.* The CDK4-pRB-E2F1 pathway controls insulin secretion. *Nat. Cell Biol.* **11**, 1017–1023 (2009).
- González-Navarro, H. *et al.* Increased dosage of Ink4-Arf protects against glucose intolerance and insulin resistance associated with aging. *Aging Cell* **12**, 102–111 (2013).
- Moreno-Asso, A., Castaño, C., Grilli, A., Novials, A. & Servitja, J.M. Glucose regulation of a cell cycle gene module is selectively lost in mouse pancreatic islets during aging. *Diabetologia* **56**, 1761–1772 (2013).

27. Abella, A. *et al.* Cdk4 promotes adipogenesis through PPAR- γ activation. *Cell Metab.* **2**, 239–249 (2005).
28. Lee, Y. *et al.* Cyclin D1–Cdk4 controls glucose metabolism independently of cell cycle progression. *Nature* **510**, 547–551 (2014).
29. Ruvinsky, I. *et al.* Ribosomal protein S6 phosphorylation is a determinant of cell size and glucose homeostasis. *Genes Dev.* **19**, 2199–2211 (2005).
30. Chicas, A. *et al.* Dissecting the unique role of the retinoblastoma tumor suppressor during cellular senescence. *Cancer Cell* **17**, 376–387 (2010).
31. Brady, C.A. *et al.* Distinct p53 transcriptional programs dictate acute DNA-damage responses and tumor suppression. *Cell* **145**, 571–583 (2011).
32. Acosta, J.C. *et al.* A complex secretory program orchestrated by the inflammasome controls paracrine senescence. *Nat. Cell Biol.* **15**, 978–990 (2013).
33. Lujambio, A. *et al.* Non-cell autonomous tumor suppression by p53. *Cell* **153**, 449–460 (2013).
34. Stolovich-Rain, M. *et al.* Weaning triggers a maturation step of pancreatic beta cells. *Dev. Cell* **32**, 535–545 (2015).
35. van Arensbergen, J. *et al.* Derepression of Polycomb targets during pancreatic organogenesis allows insulin-producing beta cells to adopt a neural gene activity program. *Genome Res.* **20**, 722–732 (2010).
36. Holland, A.M., Hale, M.A., Kagami, H., Hammer, R.E. & MacDonald, R.J. Experimental control of pancreatic development and maintenance. *Proc. Natl. Acad. Sci. USA* **99**, 12236–12241 (2002).
37. Gauthier, B.R. *et al.* PDX1 deficiency causes mitochondrial dysfunction and defective insulin secretion through TFAM suppression. *Cell Metab.* **10**, 110–118 (2009).
38. Wiederkehr, A. & Wollheim, C.B. Mitochondrial signals drive insulin secretion in the pancreatic beta cell. *Mol. Cell. Endocrinol.* **353**, 128–137 (2012).
39. Rane, S.G. *et al.* Loss of Cdk4 expression causes insulin-deficient diabetes and Cdk4 activation results in beta islet cell hyperplasia. *Nat. Genet.* **22**, 44–52 (1999).
40. Wicksteed, B. *et al.* Conditional gene targeting in mouse pancreatic beta cells: analysis of ectopic Cre transgene expression in the brain. *Diabetes* **59**, 3090–3098 (2010).
41. Scharfmann, R. *et al.* Development of a conditionally immortalized human pancreatic beta cell line. *J. Clin. Invest.* **124**, 2087–2098 (2014).
42. Morita, M. *et al.* mTORC1 controls mitochondrial activity and biogenesis through 4E-BP-dependent translational regulation. *Cell Metab.* **18**, 698–711 (2013).
43. Koyanagi, M. *et al.* Ablation of TSC2 enhances insulin secretion by increasing the number of mitochondria through activation of mTORC1. *PLoS One* **6**, e23238 (2011).
44. Fingar, D.C., Salama, S., Tsou, C., Harlow, E. & Blenis, J. Mammalian cell size is controlled by mTOR and its downstream targets S6K1 and 4EBP1-eIF4E. *Genes Dev.* **16**, 1472–1487 (2002).
45. Dor, Y., Brown, J., Martinez, O.I. & Melton, D.A. Adult pancreatic beta cells are formed by self-duplication rather than by stem cell differentiation. *Nature* **429**, 41–46 (2004).
46. Ohn, J.H. *et al.* 10-year trajectory of beta cell function and insulin sensitivity in the development of type 2 diabetes: a community-based prospective cohort study. *Lancet Diabetes Endocrinol.* **4**, 27–34 (2016).
47. Narita, M. *et al.* Rb-mediated heterochromatin formation and silencing of E2F target genes during cellular senescence. *Cell* **113**, 703–716 (2003).
48. Bandyopadhyay, D. *et al.* Dynamic assembly of chromatin complexes during cellular senescence: implications for the growth arrest of human melanocytic nevi. *Aging Cell* **6**, 577–591 (2007).
49. Chandra, T. *et al.* Global reorganization of the nuclear landscape in senescent cells. *Cell Reports* **10**, 471–483 (2015).
50. Giordano, E. *et al.* Beta cell size influences glucose-stimulated insulin secretion. *Am. J. Physiol.* **265**, C358–C364 (1993).
51. Correia-Melo, C. & Passos, J.F. Mitochondria: are they causal players in cellular senescence? *Biochim. Biophys. Acta* **1847**, 1373–1379 (2015).
52. Nicolay, B.N. *et al.* Proteomic analysis of pRb loss highlights a signature of decreased mitochondrial oxidative phosphorylation. *Genes Dev.* **29**, 1875–1889 (2015).
53. Avrahami, D. *et al.* Aging-dependent demethylation of regulatory elements correlates with chromatin state and improved beta cell function. *Cell Metab.* **22**, 619–632 (2015).
54. Ahmadian, M. *et al.* PPAR- γ signaling and metabolism: the good, the bad and the future. *Nat. Med.* **19**, 557–566 (2013).
55. Chang, J. *et al.* Clearance of senescent cells by ABT263 rejuvenates aged hematopoietic stem cells in mice. *Nat. Med.* **22**, 78–83 (2016).
56. Nardella, C., Clohessy, J.G., Alimonti, A. & Pandolfi, P.P. Pro-senescence therapy for cancer treatment. *Nat. Rev. Cancer* **11**, 503–511 (2011).
57. Turner, N.C. *et al.* Palbociclib in hormone receptor-positive advanced breast cancer. *N. Engl. J. Med.* **373**, 209–219 (2015).

ONLINE METHODS

Mice. To generate tet-inducible p16^{Ink4a} (tet-p16) mice, we conducted flippase (Flp) and flippase recognition target (*FRT*)-mediated recombination into KH2 embryonic stem cells, as previously described⁵⁸. We crossed tet-p16 and tet-*GFP* mice (mixed C57BL/6 and 129Sv background) with *Ins2*-rtTA mice⁵⁹ (ICR background) or with *Pdx1*-tTA mice³⁶ (mixed ICR background). For transgene induction using the *Ins2*-rtTA driver (tet on) we added 500 mg/L tetracycline to the drinking water of double-transgenic mice and sibling control single-transgenic mice for the indicated durations. Littermate control mice carrying either the *Ins2*-rtTA transgene only or the *Ins2*-rtTA and tet-*GFP* transgenes (as indicated in the Figures), received identical drug treatments. For induction using the *Pdx1*-tTA driver (tet off), all mice were treated with tetracycline from inception, and tetracycline was removed from drinking water to initiate p16 expression. We obtained p16-deficient mice⁶⁰ (FVB background) from the National Cancer Institute Mouse Repository. We crossed *CDK4^{+/Isl-R24C}* mice, which carry the *CDK4^{R24C}* allele preceded by a *lox-stop-lox* (*Isl*) cassette³⁹, with *MIP-CreER* mice⁴⁰ (both on mixed ICR background) and injected 6-week-old double transgenic mice with two daily doses of 8 mg tamoxifen (Sigma; 20 mg/ml in corn oil) subcutaneously to obtain beta cell-specific activation of *CDK4^{R24C}*. C57BL/6 and FVB mice were obtained from Harlan, Israel. Glucose tolerance tests and *in vivo* GSIS assays were conducted as previously described⁶¹. Fasted mice received glucose by intraperitoneal injection (2 mg per kg body weight (mg/kg)), and blood glucose or serum insulin levels were measured at the indicated time points. For insulin-tolerance tests we injected fasted mice with 0.75 units per kg body weight insulin (Humalog) intraperitoneally and measured blood glucose at the indicated time points. We conducted all experiments using sibling littermate control and experimental mice; where necessary experimental groups were comprised of multiple litters to allow statistical power. Experiments using tet-p16 mice included both males and females. We used only males in experiments with aging and p16-deficient mice, for convenience. The joint Institutional Animal Care and Use Committee of the Hebrew University and Hadassah Medical Center approved the study protocol for animal welfare. The Hebrew University is accredited by the Association for Assessment and Accreditation of Laboratory Animal Care International.

Human islets. We obtained live human islets for FACS analysis from pancreata of brain-dead subjects as previously described⁶², under approval of the Health Research Ethics Board of the University of Alberta and following informed consent. Subject details are presented in **Supplementary Table 2**. Several hundreds of islets were obtained from each donor, and these were dissociated before staining. For mRNA extraction, we obtained adult human islets from Integrated Islet Distribution program (<http://iidp.coh.org/>) as previously described^{63,64}. Adult human islets were from four female and five male donors (age, 44.7 ± 4.2 years (range, 20–60 years); body mass index, 25.02 ± 0.84 kg/m² (range, 21.2–29.1 kg/m²)). The cold-ischemia time before pancreas isolation was 12.18 ± 2.48 h. Nine normal juvenile pancreata were used in this study (6-months-old, *n* = 1; 14-month-old, *n* = 1; 20-month-old, *n* = 1; 3-year-old, *n* = 2; 4-year-old, *n* = 1; 5-year-old, *n* = 2; 9-year-old, *n* = 1) via a protocol with the National Disease Research Interchange and International Institute for the Advancement of Medicine. De-identified human islet studies were approved by the Vanderbilt Institutional Review Board.

Ex vivo glucose-stimulated insulin secretion (GSIS) assays. We isolated islets from whole pancreata using collagenase P (Roche) that was injected to the pancreatic ducts, followed by isolation on a Histopaque gradient (Sigma). Islets were incubated overnight in RPMI-1640 medium (Biological Industries) supplemented with 10% FBS, L-glutamine and penicillin-streptomycin in a 37 °C, 5% CO₂ incubator. 30–40 islets were handpicked for each assay replicate, placed in basal Krebs buffer (118 mM NaCl, 4.7 mM KCl, 1.2 mM KH₂PO₄, 1.2 mM MgSO₄, 4.2 mM NaHCO₃, 2 mM CaCl₂ and 10 mM HEPES, pH 7.4) containing 2.8 mM glucose (Sigma) and then transferred into Krebs buffer containing 16.7 mM glucose. Medium was collected after a 1-h incubation at each glucose concentration, and islets were then pelleted and solubilized. Insulin concentrations were measured by an enzyme-linked immunosorbent assay (ELISA) (Crystal Chem Inc.). Insulin concentrations in the medium

were normalized to insulin levels in the islet lysate of each sample, which is indicative of beta cell numbers. Islets from each mouse were assayed in triplicate. Where indicated, islets from three or more mice were pooled and assayed in five replicates. In the experiment in **Figure 2b**, insulin concentrations in the medium were normalized to the beta cell number in each sample (pooled from four or more mice), as scored by FACS following islet dissociation and staining for insulin.

FACS analysis. For flow cytometry analyses, we dissociated mouse or human islets into a single-cell suspension with trypsin-EDTA treatment for 5 min at 37 °C, followed by treatment with a cell fixation and permeabilization solution (BD Pharmingen). Stained cells were analyzed on a MACSQuant Analyzer (Miltenyi Biotec). For all of the mouse analyses, we pooled cells from three or more mice in each group. Human islets were analyzed independently for each subject after acquisition. Antibody staining was performed using standard procedures using antibodies to the proteins described below, as well as to: Ki67 (BD 558615; 1:50), mouse p16 (Santa Cruz sc-1207; 1:100) and Lamp2a (Abcam ab18528; 1:1,000). SA-β-Gal activity was assayed using the fluorescent β-galactosidase substrate C₁₂FDG (Invitrogen D-2893), as described⁶⁵. Briefly, we incubated dissociated islet cells with 33 μM C₁₂FDG for 1 h at 37 °C with gentle shaking and then scored fluorescent cells by FACS. For Mitotracker staining, dissociated islet cells were incubated with 200 nM MitoTracker Green (Life Technologies) for 1 h at 37 °C with gentle shaking. Cells were washed once and scored by FACS. For staining with tetramethylrhodamine ethyl ester perchlorate (TMRE), we incubated dissociated islet cells with 7 nM TMRE (Life Technologies) for 1 h at 37 °C in Krebs solution containing 3 or 20 mM glucose, with gentle shaking. For the glucose uptake assay we incubated dissociated islet cells with 2-(*N*-(7-nitrobenz-2-oxa-1,3-diazol-4-yl)amino)-2-deoxyglucose (2-NBDG) (Life Technologies, N13195) for 30 min at 37 °C in Krebs buffer containing 3 mM glucose, with gentle shaking.

Oxygen-consumption measurement. We measured real-time mitochondrial oxygen-consumption rates using the XF24 extracellular flux analyzer instrument (Seahorse Bioscience). Islets were rinsed with sodium bicarbonate-free Dulbecco's modified Eagle's medium (DMEM) supplemented with 0.5% BSA and 3 mM glucose, and 40 islets were distributed per well, with five replicate wells per group. After baseline measurements, we injected the following: glucose (20 mM), carbonyl cyanide-4-(trifluoromethoxy) phenylhydrazone (FCCP, 5 μM), and rotenone and antimycin A (5 μM). The respiratory rate of each islet sample was measured at 37 °C and analyzed. Oxygen-consumption levels were normalized to the insulin content of islets in each well and are shown relative to the value of the control islets incubated in medium with the low glucose concentration, which was defined as 1.

Tissue-section staining and analysis. We performed tissue processing for section staining as previously described⁶¹, using antibodies to the following proteins: insulin (DakoCytomation; 1:400), Ki67 (NeoMarkers RM9106S0; 1:200), Pdx1 (gift from Christopher Wright, Vanderbilt University; 1:2,500), Nkx6.1 (Beta Cell Biology Consortium; 1:500), chromogranin A (Novus NB120-15160; 1:200), human p16 (Abcam ab108349; 1:500) human p16 (BD 551153; 1:200), p21 (Santa Cruz sc-397; 1:100), pS6 (Cell Signaling 5364; 1:1,000), E-cadherin (BD Pharmingen 610182; 1:50), Atp5a (Abcam ab14748; 1:100), Cox17 (Novus NBP1-19696; 1:100) and Ndufb (Sigma HPA005640; 1:100). Secondary antibodies were purchased from Jackson ImmunoResearch Laboratories. Fluorescent images were taken on a Nikon C1 confocal microscope at 400× magnification. To calculate cell size we stained sections for E-cadherin (Cdh1) and measured cell circumference using the Image J Software. >100 cells from six mice in each group were scored. Values shown are for p16⁺ beta cells in p16-induced mice and for beta cells in control mice. To determine expression levels of p16, pS6 and mitochondrial markers in stained islet sections of human subjects, we used the NIS-Elements software (Nikon) to measure the mean intensity per section area of the fluorescent signal within islets and divided it by the mean intensity per area of the signal in the surrounding acinar tissue in the same field to account for differential staining background. >10 islets per subject were scored. For beta cell area determination, we stained paraffin-embedded tissue sections 50 μm apart, spanning the entire pancreas, for insulin and hematoxylin.

40× magnification images were obtained and merged, and the fraction of tissue stained for insulin was determined using NIS-Elements software.

RNA extraction, qRT-PCR and expression profiling. We isolated GFP⁺ cells by FACS from dissociated islets of *Ins2-rtTA;tet-GFP;tet-p16* mice and control *Ins2-rtTA;tet-GFP* mice, following tet treatment for 10 d. Total RNA was isolated by TRIzol (Invitrogen) extraction followed by RNeasy Plus Micro Kit (Qiagen), using ~50,000 beta cells from two control and three p16-expressing mice. Libraries were prepared and sequenced using Illumina's directional RNA sequencing protocol (Hi-seq). Reads were mapped using TopHat2, and quantification and normalization were done using Cuffdiff⁶⁶ to produce gene level-normalized expression values (fragments per kb of exon per million; FPKMs) and significance values. Up- and downregulated genes with $P < 0.05$ were tested for enrichment of gene sets using the hypergeometric method, using false-discovery rate (FDR) < 0.05 . Gene sets were derived from MSigDB or KEGG, or compiled from the literature as described in **Supplementary Table 1**. Total RNA extraction from human islets and qRT-PCR were performed as previously described⁶³, using the TaqMan primer-probes for *p16* (Hs00923894_m1) and *ACTB* (Hs99999903_m1) as a control, with reagents from Applied Biosystems (Foster City, CA).

Transmission electron microscopy. Islets from five mice in each group were fixed with 4% paraformaldehyde and 2.5% glutaraldehyde (EMS), post-fixed with 1% osmium tetroxide (Sigma) and dehydrated with increasing concentrations of ethanol followed by propylene oxide treatment (Sigma). For embedding we used Agar 100 resin (Agar Scientific). For imaging we stained 80-nm sections with 5% uranyl acetate for 10 min, followed by 10-min staining with lead citrate. We visualized samples with a Technai 12 Phillips transmission electron microscope equipped with a MegaView II charged-couple device (CCD) camera. To measure relative mitochondrial area we used NIS Elements software.

Mitochondrial DNA quantification. To measure mitochondrial DNA copy number, we isolated DNA from sorted GFP⁺ beta cells by standard phenol-chloroform extraction and ethanol precipitation. qPCR was used to evaluate the ratio between the mitochondrial cytochrome *b* gene (*mt-Cytb*) and the L1 repetitive element (nuclear) using the following primers sequences: *mt-Cytb*: 5'-GCAGTCATAGCCACAGCATT-3' and 5'-AAGTGGAAAGC GAAGAATCG-3', L1: 5'- GTTACAGAGACGGAGTTTGGAG-3' and 5'-CGTTTGGATGCTGATTATGGG-3'.

Western blot analysis. Protein was extracted from fresh islets by RIPA lysis buffer supplemented with the protease and phosphatase inhibitors leupeptin, aprotinin and vanadate (Sigma). Total protein concentration was determined using the Pierce BCA protein assay kit (Thermo Scientific). Antibodies used were against Pgc-1 α (Abcam ab54481; 1:2,000) and Hsp90 (Calbiochem CA1016; 1:5,000).

Human EndoC- β H2 cells. EndoC- β H2 cells were newly obtained from R. Scharfmann and Endocell, with no further authentication or testing for mycoplasma. Cells were cultured on Matrigel- and fibronectin-coated wells as

previously described⁴¹. Cells were infected with a lentivirus coexpressing *Cre* and *GFP* (Addgene #20781) or expressing *GFP* only (pRRL-GFP); in **Figure 6c** (right panel), **g,h,i** (right panel), *Cre* was expressed using the pTRIP Δ U3-CMV-nlsCre vector⁴¹, and the pLKO.1-Puro empty vector was used as a lentiviral empty vector control. For *p16* silencing a pLKO.1-Puro-shp16 was used, carrying the targeting sequence: GCATGGAGCCTTCGGCTGACT. Viruses were produced by co-transfection of backbones into 293T cells with the packaging vectors pHR8.2 and pCMV-VSV-G, followed by medium collection and centrifugal concentration. Cells were maintained for 3 weeks after infection. We performed SA- β -Gal and TMRE staining, as well as cell size and insulin secretion assays, 3 weeks after infection. SA- β -Gal staining was conducted as previously described⁶⁵. For GSIS, cells were plated 3 weeks after infection in 96-well plates at 3.5×10^4 cells/well for control cells and 7×10^4 cells/well for *Cre*-expressing cells. Seven days later, cells were incubated overnight in culture medium that contained 2.8 mM glucose and then in Krebs buffer that contained 2.8 mM glucose for 60 min. Medium was collected, and the cells were then incubated in Krebs buffer containing 16.7 mM glucose for 60 min, and the medium was collected again. Insulin levels in the medium were measured in 12 replicate wells per group by ELISA. Values were normalized to cell number in each well. For mTOR inhibition, the cells were treated with 250 nM Torin1 (Tocris) starting 3 d after infection and maintained in Torin1 for the duration of the experiment. For PPAR- γ inhibition, cells were treated with 50 μ M GW9662 (Sigma) twice a week for the duration of the experiment.

Statistical analyses. Two-sided Student's *t*-tests were used to compare mouse groups, under the assumption of normal distribution and observance of similar variance. No statistical method was used to predetermine sample size. No animals were excluded from analysis. The experiments were not randomized. There was no blinded allocation during the experiments and the outcome assessment.

58. Tokarsky-Amiel, R. *et al.* Dynamics of senescent cell formation and retention revealed by p14^{ARF} induction in the epidermis. *Cancer Res.* **73**, 2829–2839 (2013).
59. Milo-Landesman, D. *et al.* Correction of hyperglycemia in diabetic mice transplanted with reversibly immortalized pancreatic beta cells controlled by the Tet-on regulatory system. *Cell Transplant.* **10**, 645–650 (2001).
60. Sharpless, N.E. *et al.* Loss of p16^{Ink4a} with retention of p19^{Arf} predisposes mice to tumorigenesis. *Nature* **413**, 86–91 (2001).
61. Nir, T., Melton, D.A. & Dor, Y. Recovery from diabetes in mice by beta cell regeneration. *J. Clin. Invest.* **117**, 2553–2561 (2007).
62. O'Gorman, D. *et al.* Comparison of human islet isolation outcomes using a new mammalian tissue-free enzyme versus collagenase NB-1. *Transplantation* **90**, 255–259 (2010).
63. Dai, C. *et al.* Islet-enriched gene expression and glucose-induced insulin secretion in human and mouse islets. *Diabetologia* **55**, 707–718 (2012).
64. Walsh, R.M. *et al.* Improved quality of life following total pancreatectomy and auto-islet transplantation for chronic pancreatitis. *J. Gastrointest. Surg.* **16**, 1469–1477 (2012).
65. Debacq-Chainiaux, F., Erusalimsky, J.D., Campisi, J. & Toussaint, O. Protocols to detect senescence-associated β -galactosidase (SA- β -gal) activity, a biomarker of senescent cells in culture and *in vivo*. *Nat. Protoc.* **4**, 1798–1806 (2009).
66. Trapnell, C. *et al.* Differential analysis of gene regulation at transcript resolution with RNA-seq. *Nat. Biotechnol.* **31**, 46–53 (2013).